Science Advances

AAAS

advances.sciencemag.org/cgi/content/full/4/3/eaar3748/DC1

Supplementary Materials for

Earthquakes drive large-scale submarine canyon development and sediment supply to deep-ocean basins

Joshu J. Mountjoy, Jamie D. Howarth, Alan R. Orpin, Philip M. Barnes, David A. Bowden, Ashley A. Rowden, Alexandre C. G. Schimel, Caroline Holden, Huw J. Horgan, Scott D. Nodder, Jason R. Patton, Geoffroy Lamarche, Matthew Gerstenberger, Aaron Micallef, Arne Pallentin, Tim Kane

Published 14 March 2018, *Sci. Adv.* **4**, eaar3748 (2018)
DOI: 10.1126/sciadv.aar3748

This PDF file includes:

and TAN0616 (yellow filled triangles), and Van Veen grab samples collected during TAN0616 (yellow filled circles).

- table S1. Description of core facies from the Kaikōura Canyon and the Hikurangi Channel, levee, and trough.
- table S2. Metadata for multicores collected along the Kaikōura Canyon and the Hikurangi Channel, levee, and trough.
- table S3. Results of ^{234}Th measurements and excess ^{234}Th ($^{234}Th_{ex}$) activities reported in the text.
- table S4. Volume budget calculation details, with lower-bound estimates shown in parentheses.
- References (*34*–*38*)

Supplementary Material

Sedimentology

The eight multicores provide insights into the presence/absence of deposits formed by the sediment density flow triggered by the Kaikōura earthquake and informs the spatial extent of this flow down the Hikurangi Channel system. All cores located in the Kaikōura Canyon and Hikurangi channel, levee and trough contained a recently emplaced turbidite as the youngest, surficial deposit in the cores that ranged in thickness from 5 cm to 65 cm (fig. S1). The sedimentary and hence flow characteristics of the deposit varied between depositional settings and with distance down-channel from the source region in the Kaikōura Canyon.

The stratigraphy of the recent flow deposit was most complex in the cores from the axis of the Kaikōura Canyon (TAN1701_181 and TAN1701_182). Here the deposits are characterised by a muddy debrite (Dm-2, classification of facies after (*34*); fig. S1) that contains isolated, pebble-sized lithic clasts and is overlain by a sandy turbidite. The upper contact of the debrite is sharp and exhibits flutes consistent with an erosional contact between the debrite and turbidite beds. In the canyon axis, the overlying turbidite is 20 cm thick and is composed of multiple (multi-pulsed), fining-upwards sequences of planar laminated, medium to fine sands (Tb-2). These units fine upwards into a 10 cm-thick, normally graded mud unit (Te-2) (fig. S1 and table S1). The combination of Dm-2, Tb-2 and Te-2 facies suggest a range of flow processes were involved in depositing sediment in the canyon axis during the co-seismic event. This sediment density flow event started with a cohesive debris flow that likely originated from canyon head mass-wasting that deposited the debrite unit. This was followed by a high-density turbidity current that deposited laminated, medium to fine sands (Tb-2) that transitioned with time into a low-density turbulent suspension that deposited the muddy turbidite tail (Te-2).

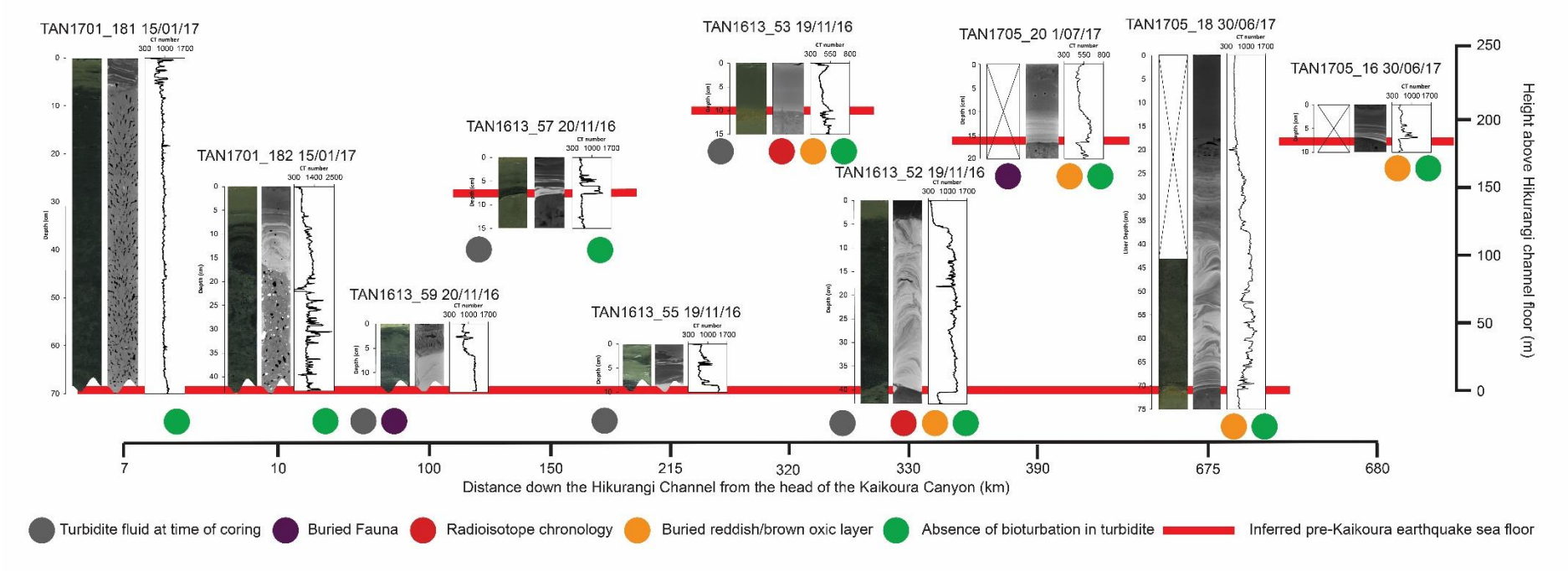

fig. S1. Image, CT slice, and CT number (a bulk density proxy) for cores that contain recently emplaced graded deposits from the Kaikōura Canyon and the Hikurangi Channel and its levee and overbank regions.

table S1. Description of core facies from the Kaikōura Canyon and the Hikurangi Channel, levee, and trough.

Lithofacies	Description	Classification*	Interpretation
A	>300 mm-thick beds of massive, fine sandy mud that contains isolated, pebble-sized lithic clasts that have A axis diameters of up to 10 mm.	D_{m-2}	Debrite formed by deposition of subaqueous debris flow sediments.
B	Up to 100 mm-thick beds of planar laminated, medium to fine sand.	T_{B-2}	Turbidite bed formed by repeated collapse of near-bed laminar shear layers within high-concentration flows
C	Up to 300 mm-thick beds of convoluted, ripple cross-laminated, medium to fine sand.	T_C	Turbidite bed formed by low rates of settling from a low-density fully turbulent flow
D	Up to 200 mm-thick, planar laminated, normally graded or homogenous mud.	T_{E-1}, T_{E-2} or T_{E-3}	Turbidite bed formed by suspension settling from a muddy turbulent flow

*Turbidite classification after (*34*).

In the floor of the Hikurangi Channel (TAN1613_52, 55, 59 and TAN1705_17), the turbidite has a decimetre thick basal unit of convoluted, ripple cross-laminated, medium to fine sands (Tc) (Fig. 2 and fig. S1). A distinct grainsize break generally occurs at the top of the sand beds, which are overlain by 5-40 cm thick mud units (Te-1, Te-2 or Te-3). The medium to fine sands were likely deposited from a low-density sandy turbidity current. The grainsize break between Tc and Te units record bypass of intermediate grainsizes before deposition of the muddy turbidite tail through suspension settling from a lower velocity, muddy turbidity current.

On the Hikurangi Channel levee and trough (TAN1613_53, 57 and TAN1705_16, 20), up to 250 metres above the channel floor, the turbidite is composed of a predominantly planar laminated, normally graded or homogenous mud unit (Te-2 or Te-3) (fig. S1 and table S1). The location of these core sites hundreds of meters above the channel floor mean their deposits provide insights into the local flow height and nature of the upper part of the turbidity current. The muddy turbidites were likely deposited through suspension settling from a lower velocity muddy turbulent suspension that characterised the upper parts of the turbidity current. Importantly, the levee and trough core sites demonstrate that flow must have exceeded 250 m in height at 300 km from the source and was more than 180 m in height at our most distal core site, 680 km from the source. Hence, the flow likely propagated far beyond 680 km down the Hikurangi Channel, potentially into the deep Southwest Pacific Ocean.

Together, the deposits in the canyon, channel, levee and trough cores are consistent with a sediment density flow that involved a complex series of flow processes close to source as material liberated from subaqueous slopes by mass-wasting evolved into cohesive debris flows. With time and distance down-canyon these evolved into a high-density turbidity current and finally a low-density turbidity current that travelled at least 680 km north along the Hikurangi Channel and had flow heights exceeding 250 m.

Chronology

Multiple lines of evidence support very recent emplacement of the turbidite. The turbidite was highly fluidized in cores taken within days of the Kaikōura earthquake (sampled between 18-30th November) from both the Hikurangi channel and levee. The fluidized nature of both coarse- and fine-grained turbidite beds was further

demonstrated by the decrease in turbidite thickness in cores by up to half due to dewatering and settling in the months following sampling (table S2). These observations suggest the deposits were still settling at the time of initial sampling, only days after the earthquake. Fresh biological remains of gut and shell from the echinoderms *Brissopsis oldhami* and *Holanthus expergitus* were found at a depth of 14-18 cm in fluidized sands from the base of the turbidite in core TAN1613-59 located in the Hikurangi Channel at a water depth of 2386 m (table S1 and table S2). *Brissopsis oldhami* occupies a niche on the seabed between 660 m and 2199 m water depth suggesting the remains identified in the cores were carried to the core site by the flow and emplaced decimetres below the surface. Un-decayed echinoderm gut in turbidite sediments supports emplacement immediately prior to coring.

table S2. Metadata for multicores collected along the Kaikōura Canyon and the Hikurangi Channel, levee, and trough.

Station	Site Name	Date (NZDT)	Water Depth (m)	Latitude (decimal degrees, °)	Longitude (decimal degrees, °)	Recent turbidite	Turbidite thickness at time of coring (cm)	Settled turbidite thickness (cm)	Change in turbidite thickness (cm)	Oxic layer underlying turbidite	Bioturbation in turbidite	Radionuclide evidence for recent emplacement
TAN1701_181	K100	15/01/2017	1046	-42.501	173.625	Yes	6	N/A	N/A	No	No	N/A
TAN1701_182	K94	15/01/2017	1186	-42.492	173.653	Yes	20	N/A	N/A	No	No	N/A
TAN1613_59	Hik2	20/11/2016	2386	-42.470	174.491	Yes	20	14	6	No	No	N/A
TAN1613_55	Hik7	19/11/2016	2750	-42.236	175.708	Yes	18	N/A	10	No	No	N/A
TAN1613_57	Hik4	20/11/2016	2439	-42.233	174.965	Yes	14	8	6	No	No	N/A
TAN1613_61	Marl2	20/11/2016	1150	-42.099	174.489	No	N/A	N/A	N/A	N/A	N/A	No
TAN1613_52	Hik20	19/11/2016	2969	-42.096	176.801	Yes	53	40	13	No	Yes	Yes
TAN1613_53	Hik21	19/11/2016	2733	-41.999	176.501	Yes	20	10	10	Yes	No	Yes
TAN1705_20	Hik9	1/07/2017	2874	-41.687	176.983	Yes	18	N/A	N/A	Yes	No	N/A
TAN1705_17	Hik18	30/06/2017	3410	-40.163	178.940	Yes	65	N/A	N/A	Yes	No	N/A
TAN1705_16	Hik16	30/06/2017	3234	-40.123	178.809	Yes	7	N/A	N/A	Yes	No	N/A

Sedimentological evidence for recent emplacement of the uppermost turbidite at the seafloor is provided by the reddish brown oxic layer that underlies the deposit in both the channel and levee cores. This oxic layer is characteristic of undisturbed seafloor where sediments have been at the sediment-water interface and subject to biological activity for extended periods (months to years. The absence of oxic layers at the sediment-water interface in cores that contain turbidites at core tops provides further evidence for recent emplacement because oxic layers develop rapidly (<2 years) in high deposition rate settings (*35*). Turbidite deposits at the top of each core exhibit no evidence of bioturbation, which contrasts with the highly bioturbated underlying sediments that include older turbidite beds (Fig. 2). The lack of bioturbation suggests insufficient time has elapsed following turbidite deposition to allow for colonisation and reworking of the sediments by benthic organisms.

Excess ^{234}Th was measured in cores TAN1613_53 from the channel levee, TAN1613_52 from the channel axis and TAN1613_61 from an undisturbed site in a Marlborough slope basin (table S3). 20-100 Bq.kg^{-1} of excess ^{234}Th activity was present in turbidite sediments from both TAN1613-53 and TAN1613-52 (Fig. 2). The highest levels of excess ^{234}Th activity that were greater than 480 Bq.kg^{-1} were detected in the oxic layers beneath the silty turbidite in core TAN1613_53 and at the sediment-water interface in the undisturbed slope basin core TAN1613_61 (Fig. 2; table S3). High levels of excess ^{234}Th activity in the turbidite sediment and the underlying oxidized layer provide unequivocal evidence of recent emplacement at the time of coring 4 days after the Kaikōura earthquake. The absence of excess ^{234}Th activity below the turbidite in core TAN1613_52 from the channel axis is consistent with the sharp, fluted erosional contact between the base of the turbidite and underlying sediments.

table S3. Results of ^{234}Th measurements and excess ^{234}Th ($^{234}Th_{ex}$) activities reported in the text.

Depth down settled core (cm)	Sample number	Client Code	Counting date	^{234}Th (Bq.kg^{-1})	Counting date	^{234}Th (Bq.kg^{-1})	Reference Date	$^{234}Th_{ex}$ (Bq.kg^{-1})
0.5	2016-2251	TAN1613_52 HIK20 0 - 1 cm	16/12/2016	49 ± 14	5/04/2017	18 ± 16	14/11/2016	98 ± 48
15	2016-2252	TAN1613_52 HIK20 14 - 16 cm	16/12/2016	30.6 ± 7.7	3/04/2017	30.4 ± 7.8	14/11/2016	31 ± 25
41	2016-2253	TAN1613_52 HIK20 40 - 42 cm	20/12/2016	21.2 ± 5.6	3/04/2017	21.4 ± 5.4	14/11/2016	21 ± 21
0.2	2016-2254	TAN1613_53 HIK21 0 - 1 cm	5/01/2017	61 ± 16	7/04/2017	38 ± 11	14/11/2016	147 ± 89
3.8	2016-2256	TAN1613_53 HIK21 9 - 10 cm	5/01/2017	57 ± 15	10/03/2017	37 ± 10	14/11/2016	139 ± 89
6.3	2016-2257	TAN1613_53 HIK21 15.5 - 16 cm	20/12/2016	65 ± 17	10/03/2017	43 ± 12	14/11/2016	109 ± 59
7.5	2016-2258	TAN1613_53 HIK21 18 - 18.5 cm	30/12/2016	58 ± 15	14/03/2017	43 ± 11	14/11/2016	105 ± 73
8.3	2016-2259	TAN1613_53 HIK21 20.5 - 21 cm	30/12/2016	68 ± 17	10/03/2017	43 ± 11	14/11/2016	147 ± 82
8.7	2016-2261	TAN1613_53 HIK21 21.5 - 22 cm	14/12/2016	84 ± 22	14/03/2017	47 ± 13	14/11/2016	139 ± 60
9.1	2016-2263	TAN1613_53 HIK21 22.5 - 23 cm	14/12/2016	90 ± 23	14/03/2017	47 ± 13	14/11/2016	154 ± 62
9.3	2016-2264	TAN1613_53 HIK21 23 - 23.5 cm	14/12/2016	83 ± 21	10/03/2017	29.9 ± 8.6	14/11/2016	162 ± 55
9.5	2016-2265	TAN1613_53 HIK21 23.5 - 24 cm	14/12/2016	114 ± 29	14/03/2017	43 ± 12	14/11/2016	219 ± 76

10	2016-2266	TAN1613_53 HIK21 24 - 24.5 cm	14/12/2016	224 ± 56	17/03/2017	51 ± 13	14/11/2016	480 ± 140
10.5	2016-2267	TAN1613_53 HIK 21 24.5 - 25 cm	30/12/2106	72 ± 18	17/03/2017	41 ± 11	14/11/2016	168 ± 83
11	2016-2268	TAN1613_53 HIK21 25 - 25.5 cm	30/12/2016	41 ± 11	14/03/2017	33 ± 10	14/11/2016	66 ± 58
11.5	2016-2269	TAN1613_53 HIK21 25.5 - 26 cm	30/12/2016	55 ± 14	10/03/2017	38 ± 11	14/11/2016	109 ± 71
0.5	2016-2280	TAN1613_61 MARL2 0 - 1cm	11/01/2017	242 ± 60	7/04/2017	51 ± 14	14/11/2016	1140 ± 350
1.5	2016-2281	TAN1613_61 MARL2 1 - 2 cm	12/01/2017	97 ± 24	7/04/2017	31.8 ± 8.6	14/11/2016	420 ± 150
2.5	2016-2282	TAN1613_61 MARL2 2 - 3 cm	12/01/2017	40 ± 10	30/03/2017	31.1 ± 8.1	14/11/2016	90 ± 67
3.5	2016-2283	TAN1613_61 MARL2 3 - 4 cm	20/01/2017	47 ± 12	5/04/2017	39 ± 10	14/11/2016	100 ± 120

Sediment volume budget analysis

Our analysis reveals the system is dominated by substantial erosion, matching the geomorphic observations. Deposition in the system is minimal in comparison. It is likely that there is local deposition at a scale of meters that is not represented on fig. S2 because it is overwhelmed by the erosion signature. Deposition is apparent at the canyon rim in fig. S2 due to uplift of the shelf by the Hundalee Fault. The largest individual landslides at the canyon rim were approximately 1 x 10^6 m^3. The total amount of material derived from the canyon rim is minor in comparison to the amount of material mobilised in the upper canyons (e.g. Haumuri and Kaikoura in fig. S2). The majority of the eroded volume comes from the upper canyon where uncertainty is relatively low (fig. S2). We acknowledge high uncertainty in the lowermost reach of the canyon (alternating pink and blue in fig. S2 *cf.* green and red in fig. S2) but this does not have a significant impact on the sediment budget calculations. We account for this uncertainty using the Limit of Detection method described in the Materials and Methods section. Figure S3 shows an area of the canyon where TOPAS sub-bottom profiler data shows an opaque surface lobe of sediment that matches an area of deposition within a zone of erosional change that we interpret as a fresh deposit associated with canyon flushing. The good correlation with the TOPAS seismic data validates the multibeam difference analysis.

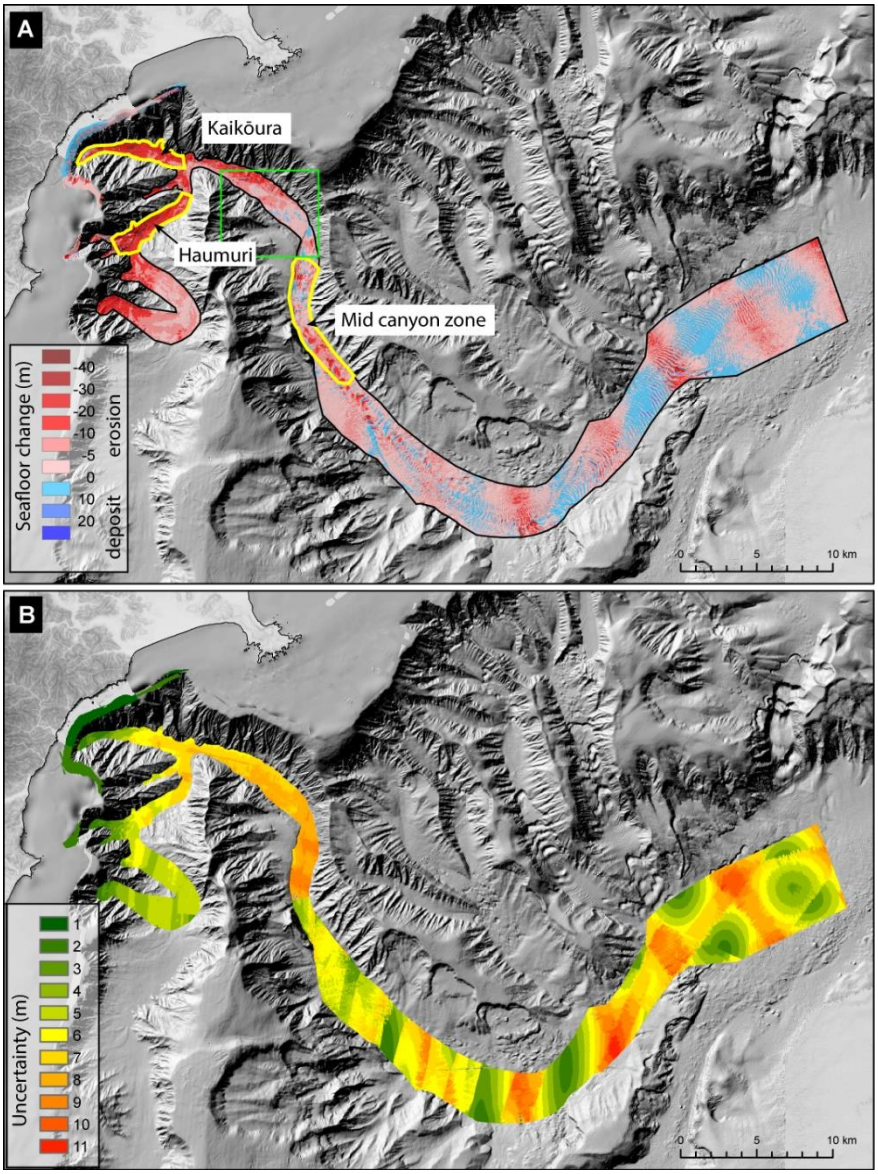

fig. S2. Difference between the pre- and post-earthquake DEMs (color-coded with erosion in red and deposition in blue), overlaid on the shaded bathymetry (grayscale). (**A**) The different zones for which analysis has been carried out are also delineated in yellow and labeled. Haumuri and Kaikōura refer to the specific canyon heads of the Kaikōura Canyon system. Green rectangle shows the extent of fig. S3. (**B**) Combined uncertainty for the difference of DEMs, propagated in quadrature from the DEMs' individual uncertainty.

table S4. Volume budget calculation details, with lower-bound estimates shown in parentheses. "Upper canyon" and "mid canyon" refers to the areas within yellow polygons in fig. S2.

	Area (m^2)	Erosion (m^3)	Deposition (m^3)	Volume net change (m^3)
All canyon floor	2.20E+08	-1.04E+09 (-4.06E+08)	1.07E+08(1.05E+07)	-9.35E+08(-3.95E+08)
Upper canyon	1.23E+07	-2.18E+08(-1.94E+08)	2.02E+06(1.61E+06)	-2.16E+08(-1.92E+08)
Mid canyon	1.13E+07	-6.30E+07(-2.05E+07)	2.60E+06(1.49E+05)	-6.04E+07(-2.04E+07)

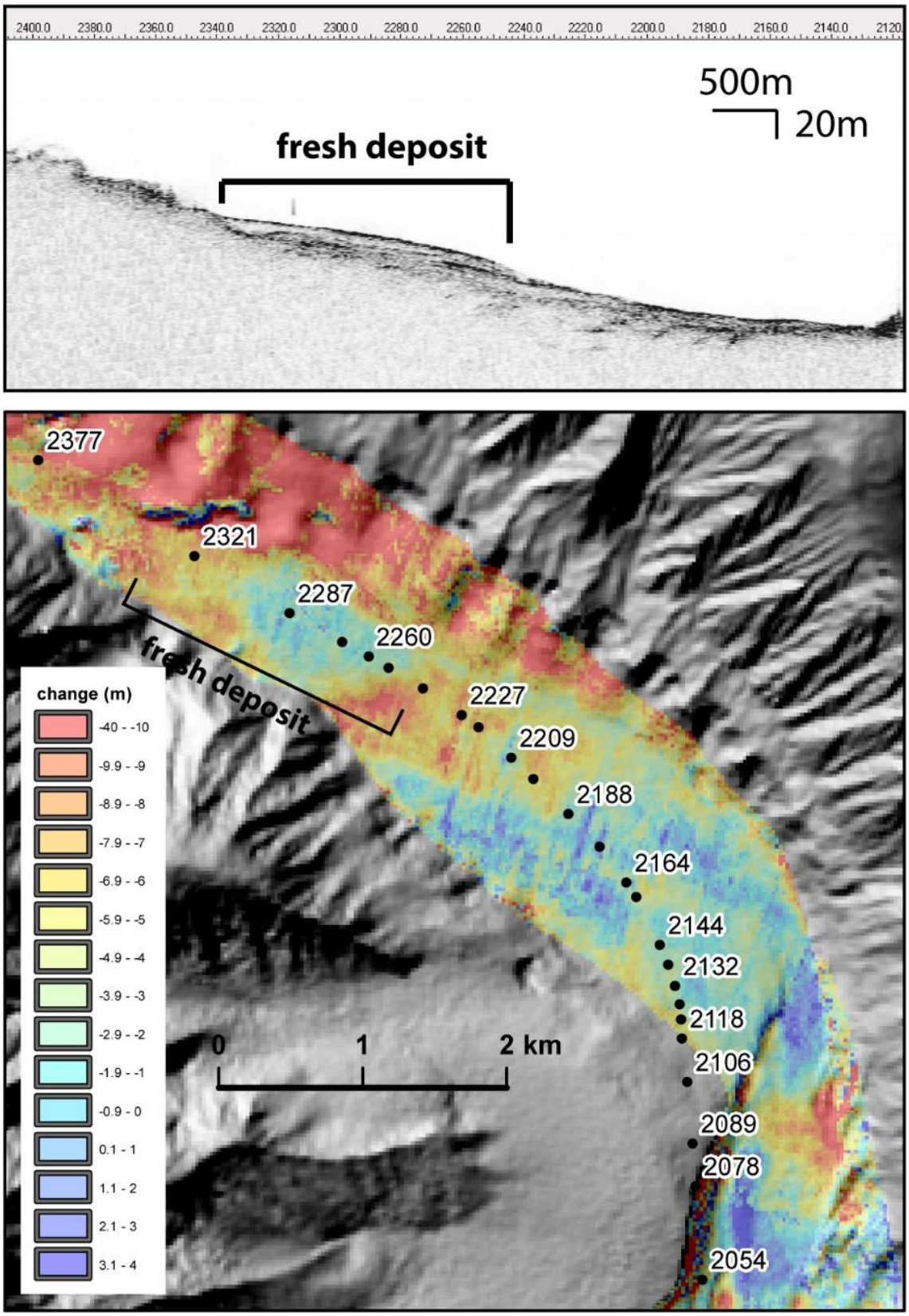

fig. S3. Localized deposition in the mid-canyon region as validation for difference analysis. Top panel: TOPAS high-resolution seismic reflection sub-bottom profile showing a transparent lobe interpreted as a fresh deposit related to the earthquake. Lower panel: Multibeam difference map of the area. Note the good correlation between the longitudinal distribution of deposition from point 2227 and 2321 on the TOPAS profile. Location of map indicated on fig. S2.

Ground motion modeling and recurrence interval estimate

The pattern of co-seismic landsliding within the Kaikōura Canyon provides an opportunity to estimate the threshold ground motions required to trigger co-seismic failure of the canyon rim. Landsliding on the canyon rim occurs in a concentric arc around the rupture tip of the Hundalee Fault (fig. S4). Importantly, there is a clear demarcation between landslide triggering to no triggering north and south of the Hundalee Fault. We model peak ground acceleration (PGA) as a measure of ground motion known to correlate with the spatial distribution of landsliding. PGA was modelled using the McVerry 2006 ground-motion prediction equation (GMPE) (*19*). We chose this particular GMPE over more recent updates because it is the one used in the current version of the New Zealand National Seismic Hazard model (NSHM) (*23*). Consistency with the NSHM is important because the model was used to estimate the recurrence interval of canyon flushing.

GMPE modelling requires an earthquake source to be defined in the form of a fault source geometry, focal depth and earthquake magnitude (*19*). The November 16th M_w7.8 Kaikōura earthquake involved rupture on at least 21 individual faults. Hence, the total moment (M_w7.8) of the earthquake is the sum of smaller rupture sources associated with each ruptured fault, with near-field ground motions dominated by proximity to the individual ruptured faults (*13*). During the earthquake, the Hundalee and Point Kean faults ruptured in close proximity to the head of the Kaikōura and Haumuri canyons and are assumed here to be the source of PGA at the canyon heads. The geometry and extent of rupture on the Hundalee Fault is well constrained by both on- and offshore mapping, whereas the Point Kean Fault geometry is only inferred based on the pattern of coastal deformation (*14*) and was absent in the original published source model of (*13*). Given the uncertainty about the geometry and even the existence of the Point Kean Fault source, we model two ground-motion scenarios and select the most probable based on comparison to the KIKS strong ground motion station located on the Kaikōura Peninsula (fig. S4).

The fault source scenarios were modelled using magnitude and geometry defined by the latest and most detailed published source model for the Kaikōura earthquake (*14*). The first scenario involves only the Hundadee Fault, which has an oblique mechanism, a homogenous slip distribution, a strike of 250°, length of 20 km, and a M_w of 7.05. The second source scenario has both the Hundalee Fault and the Point Kean Fault defined as a source with a thrust mechanism, homogenous slip distribution, strike of 235°, length of 38 km and a M_w of 7.2. We used comparison between the predicted and observed PGA at the KIKS strong ground motion station to select the most realistic PGA model. For consistent comparison between observed and modelled PGA we used a used site class B, bedrock, because the KIKS station is installed on a bedrock substrate.

Our preferred scenario to estimate PGA thresholds for co-seismic landsliding on the canyon rim is the single Hundalee rupture for the following reasons:

- The GMPE predicts 0.26g at the KIKS station which is in good agreement with the observed PGA of 0.25g. Conversely, the combined Hundalee and Point Kean source scenario models a PGA of 0.45g at the KIKS station, which is nearly twice the value of the observed PGA.
- The acceleration time history for the KIKS station also shows that the PGA was reached only once during the rupture. As the Hundalee and Point Kean faults likely ruptured at different times during the earthquake and the Hundalee fault source is well -constrained by multiple kinematic models therefore observed PGA most likely driven by Hundalee rupture (*36*)
- The Point Kean source is about 15 km further north than the simple homogenous slip source in this model, suggesting smaller PGA values driven by Point Kean fault in the canyon (*36*)

The Kaikōura Canyon failures nucleated in sediments with characteristics equivalent to site class C, shallow soils >20 m deep. Hence site class C was used when modelling PGA for comparison to the spatial extent of canyon rim landsliding.

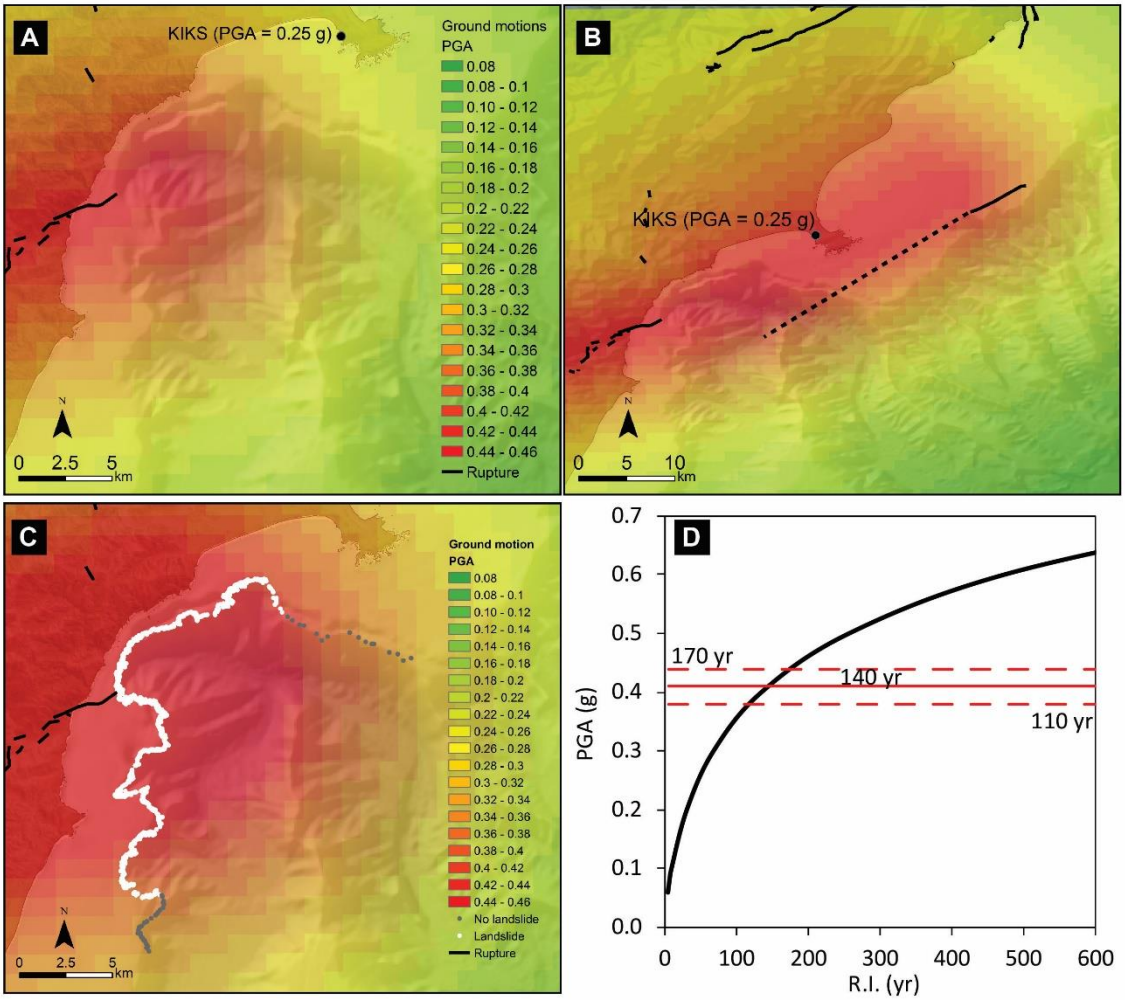

fig. S4. Ground motion modeling and recurrence interval estimate for canyon flushing triggered by widespread failure of the Kaikōura Canyon rim. The Hundalee Fault (**A**) and the Hundalee and Point Kean faults (**B**) scenarios using the GMPE for site class B, bedrock, suitable for comparison to the observed PGA at the KIKS strong ground motion station on the Kaikōura Peninsula. (**C**) Comparison of ground-motion simulation for the Hundalee Fault using the GMPE for site class C (12) and the distribution of landsliding on the canyon rim triggered by the Kaikōura earthquake. (**D**) Hazard curve derived from the Kaikōura Canyon from the NSHM used to derived recurrence interval estimates for PGA.

A recurrence interval (R.I.) for widespread canyon-rim landsliding that we infer initiates canyon flushing sediment flows was generated by comparing the threshold motions with hazard curves produced from the NSHM. The NSHM was used to generate the relationship between PGA and recurrence interval for the Kaikōura canyon assuming site class C for the offshore canyon-rim sediments (*23*).

Comparison between modelled PGA for the Kaikōura canyon and the distribution of canyon-rim landsliding reveals a very similar PGA threshold for the transition between landsliding and no landsliding at the northern and southern extents of the landslide distribution. The southern transition occurs at the 0.38g PGA contour, while the northern transition occurs at the 0.44g PGA contour. On this basis, the threshold PGA for triggering extensive canyon rim landsliding that we infer initiates canyon flushing flows has a value of 0.41 ± 0.03 g (fig. S4). Based on the PGA vs recurrence interval hazard curve for the Kaikōura Canyon derived from the NSHM, these threshold motions have a recurrence interval of 140±30 years. This recurrence interval agrees well with the 160 year inter-event time suggested by Lewis and Barnes (*16*) on the basis of a radiocarbon-dated gravel turbidites retrieved from the axis of the Kaikōura Canyon.

Canyon geomorphic change analysis

Mid-canyon incision from this canyon flushing event

We define an area of exposed canyon substrate (i.e. an area of the canyon floor where there is no significant sediment fill – the mid-canyon zone in fig. S2) based on: (1) geomorphology characteristic of substrate scour, (2) unsuccessful coring attempts in this region indicating hard material, (3) high reflectivity backscatter indicating the upper limit of coarse sediment armouring in the lower canyon, and (4) towed camera observations that show irregular rocky substrates in the canyon floor. Bedrock substrate in this canyon is known to be a combination of Mesozoic greywacke (sandstone and argillite) and Neogene limestone and mudstone. This mid-canyon zone is shown in fig. S2, and the area and magnitude of canyon change is shown in table S4. We calculate a spatially averaged erosion depth of 5.6 m with a Limit of Detection value of 1.8 m. We use the recurrence interval for canyon flushing to calculate an annual incision rate of 40±11 (13±3) mm.yr^{-1}.

Long-term canyon downcutting

We use our localised incision rate to project what the long-term downcutting rate is for this canyon. We make the assumption that the long term uplift of 1.1±0.1 mm.yr^{-1} recorded from marine terraces at Kaikoura Peninsula (*33*) is appropriate across the canyon region. We assume that spatial distribution and magnitude of localised incision derived for this canyon flushing event is characteristic of the long-term incision and that the location of incision will occur at different locations in the canyon axis through time and over millennial timescales that affect the full length of the canyon axis.
We calculate a long-term incision rate $I_{longterm}$ (mm.yr^{-1}) as

$$I_{longterm} = \left(\frac{Ilocal}{\left(\frac{Ptotal}{Plocal}\right)T} \right) - U$$

P_{total} = the total canyon profile length (m); P_{local} = the local canyon profile length affected by incision during canon flushing (m); I_{local} = the local incision rate during canyon flushing (mm); T = event recurrence (yrs); U = uplift (mm/yr)

From this equation, we calculate a preferred long-term incision rate of 6.4 m.kyr^{-1} with a minimum of 0.8 m.kyr^{-1} and maximum of 8.9 m.kyr^{-1}, derived by propagating uncertainties from the amount of incision, uplift rate and event recurrence intervals This would mean that to incise a 1000 m-deep canyon would take in the order of 156 kyrs, but might as much as 1200 kyrs assuming the lower rate.

Coarse sediment bedform movement

The lower region of the Kaikōura Canyon floor has been recognised as containing coarse sediment bedforms from a strong acoustic backscatter signal, and from well-rounded, cobble- and boulder-sized gravel material recovered in sediment cores (*16*). The correlation between the cores and backscatter indicates that coarse clastic sediments are the predominant material type in the lower canyon.

Pre- and post-earthquake multibeam imaging demonstrates that the coarse sediment bedforms have significantly changed. This is apparent from examining shaded relief maps derived from digital elevation models (refer to links at beginning of Supplementary Material) and the multibeam difference analysis. Profiles over bedforms show that these are relatively symmetrical in terms of lee and stoss gradients characteristic of large sediment wave or sediment dunes rather than cyclic steps (*37*). It is apparent that these coarse sediment bedforms have moved down the canyon in a coherent fashion, i.e. they have maintained their same planform arrangement.

To analyse the spatial extent of bedform movement and quantify the magnitude of coherent displacement we used digital image correlation techniques implemented in COSI-corr (*20*). Image correlation was applied to the slope magnitude of repeat bathymetry data. Correlation of 1600 m by 1600 m patches (64 by 64 pixels) was undertaken on a 400 m grid. Minimal manual data editing was conducted to remove erroneous signal introduced by data gaps. Figure S5 shows the mean displacement vectors down the lower canyon axis and subsets of local displacement vectors. Compass diagrams show consistent movement in sections 1-5 with vector direction mostly within 30° of each other (fig. S5). Displacement vectors outside of the canyon are negligible and randomly oriented. It is clear that the sediment waves have translated down canyon by up to 500 m in sections 1,2 and 4. Vector orientation in section 6 is less consistent spatially than further up canyon.

The mechanism for this movement is most likely bedload traction and migration (*38*); however, coherent down-canyon bedform movement has also been proposed to be facilitated by deep-seated failure and glacier-like movement in canyon fill (*24*). We do not have sufficient data to resolve this here but consider this a key topic for future research.

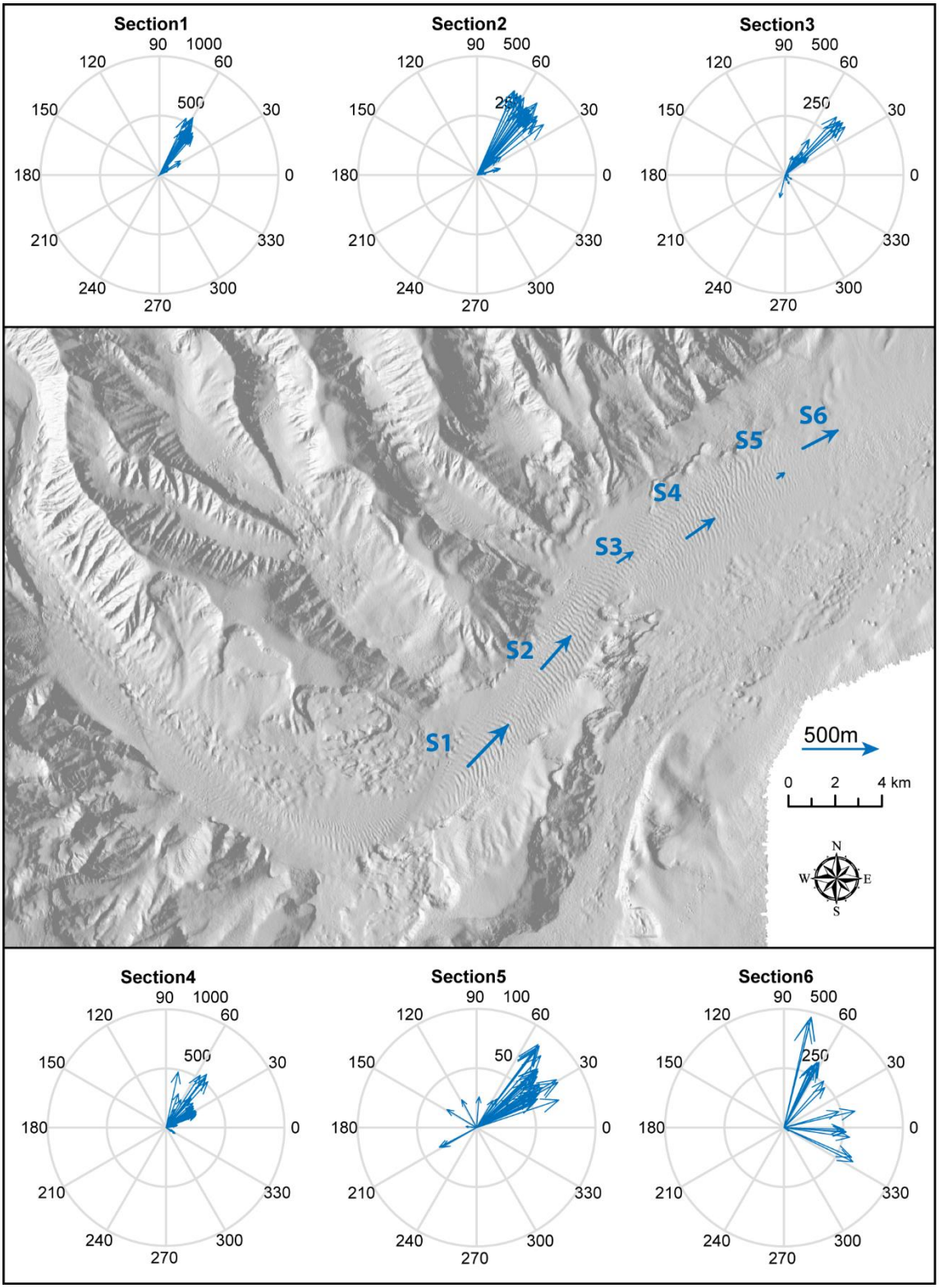

fig. S5. Mean co-registration of optically sensed images and correlation (COSI-corr) results for sediment wave movement with detailed results plotted as compass diagrams by sector. Figure extent as for Fig. 3.

Biology

Detailed methods, results, and discussion of pre-earthquake photographic transects and seabed samples collected in 2006 during RV *Tangaroa* voyage TAN0616 are already published (*17*) (fig. S6). The camera system used at this time was the same as used in the post-earthquake surveys (i.e. NIWA's Deep Towed Imaging System, DTIS) in February 2017 but both video and still image camera specifications have changed between surveys. On 1 February 2017, RV *Tangaroa* voyage TAN1701 diverted to Kaikōura Canyon to re-survey DTIS photographic transects originally surveyed during TAN0616 and collect sediment cores (Ocean Instruments MC-800 multicorer) at sites along these transects (fig. S6).

DTIS is a battery-powered towed camera frame deployed on a single-conductor cable with real-time video feed and control of camera and light functions via a modem link. In its 2017 configuration, DTIS recorded continuous high definition digital video (Sony HDRP J790P, HD1080p), with high resolution digital still images (Nikon D3200 SLR, 24 megapixel JPEG) captured simultaneously at 15 second intervals throughout the transect. Video lighting was from two 150W LED floodlight units (Sealite Sphere 5105, Sea & Sea Inc.), and stills lighting from 2 x 330W strobe units (Develogic Gmbh).

DTIS transects were run at 0.6 knots (0.3 ms^{-1}) at a target altitude of 2-3 m above the seafloor, using RV *Tangaroa*'s Dynamic Positioning system (DP) to maintain precise control of course and speed over the ground. In this altitude range, image frame width at the seabed is approximately 3 m. Full resolution video and still images were recorded at the seabed and downloaded on return to the surface. The low-resolution video image transmitted to the surface in real-time enabled control of camera altitude and initial evaluation of seabed substratum types and fauna. The seabed position of DTIS was monitored by an acoustic ultra-short baseline (USBL) transponder system (Kongsberg HiPAP) and plotted in real time using Ocean Floor Observation Protocol software (OFOP, http://www.ofop-by-sams.eu/). Transects were run as closely as possible along the seabed tracks of transects first surveyed in 2006, by reference to USBL navigation data recorded in OFOP log files from voyage TAN0616 to guide deployments. Estimated precision of the USBL position at 1000 m depth is ±3 m.

Observations of seabed substrata and individual benthic and demersal fauna, including fishes, and bioturbation marks were recorded using OFOP throughout all camera deployments. After deployment, image files were downloaded and both video and still imagery were reviewed at full resolution to identify benthic fauna.

Five of the eight TAN0616 DTIS transects in the canyon were re-surveyed successfully, capturing 5 hours 50 minutes of seabed video (approximately 6 linear kilometers) with 1390 high-resolution still images (fig. S6). Two multicorer deployments were completed, collecting eight sediment cores in total (TAN1701_181 and 182).

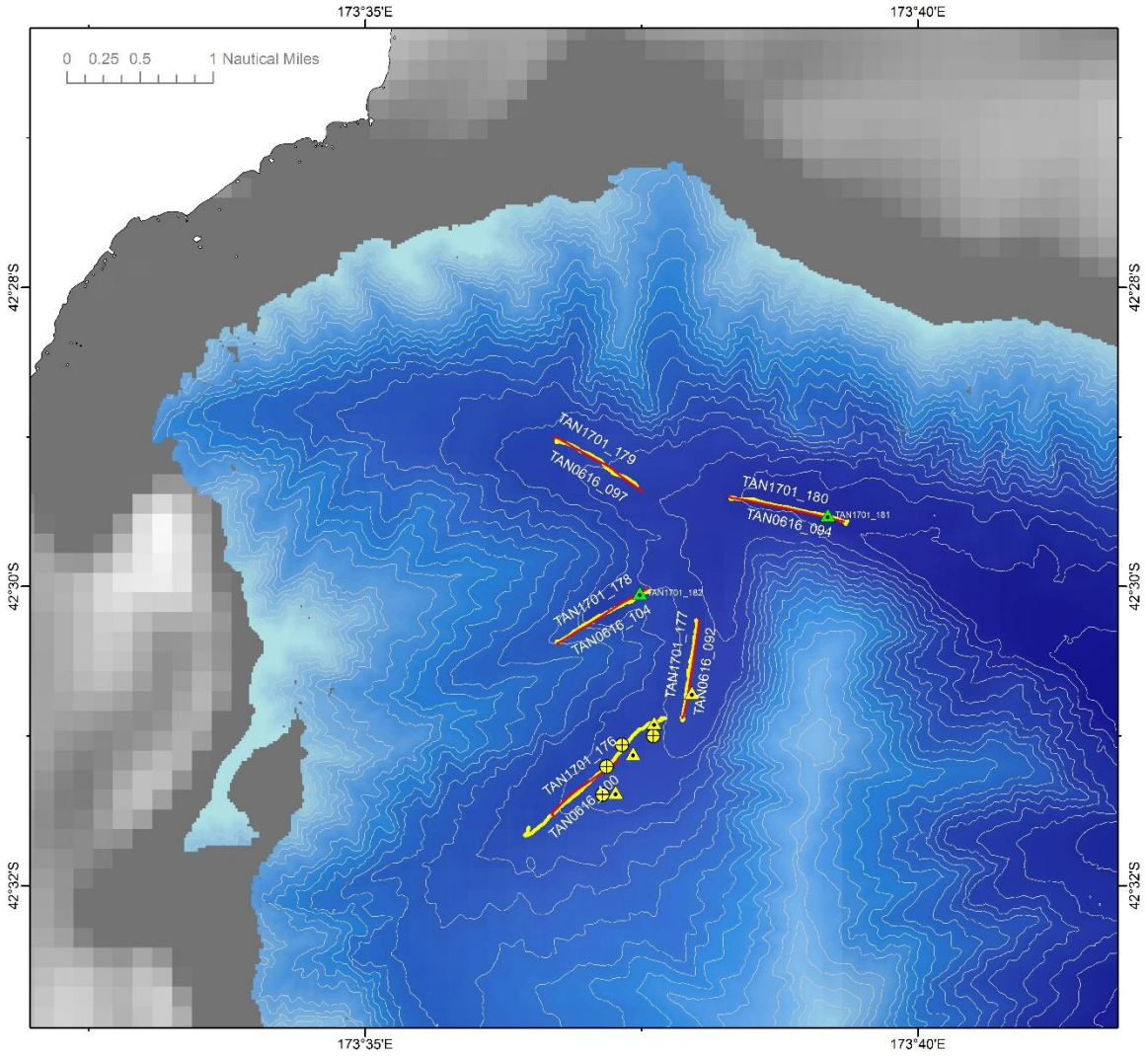

fig. S6. The Kaikōura Canyon head showing the location of deep-towed imaging system (DTIS) camera transects run during TAN1701 (red lines) and TAN0616 (yellow lines), multicore deployments during TAN1701 (green filled triangles) and TAN0616 (yellow filled triangles), and Van Veen grab samples collected during TAN0616 (yellow filled circles). Note, the multibeam bathymetry data used to illustrate seabed topography here do not show changes resulting from the November 2016 Kaikōura Earthquake.